AIAA 97-2718
Modeling of a Rijke-Tube Pulse Combustor Using Computational Fluid Dynamics

B. Entezam and W. K. Van Moorhem
University of Utah
Salt Lake City, UT 84112

J. Majdalani
Marquette University
Milwaukee, WI 53233

33rd AIAA/ASME/SAE/ASEE Joint Propulsion Conference and Exhibit
6–9 July 1997
Seattle, WA

MODELING OF A RIJKE-TUBE PULSE COMBUSTOR USING COMPUTATIONAL FLUID DYNAMICS

B. Entezam* and W. K. Van Moorhem†
University of Utah, Salt Lake City, UT 84112
and
J. Majdalani‡
Marquette University, Milwaukee, WI 53233

Abstract

A computational fluid dynamics (CFD) technique is used to investigate the unsteady flowfield inside a Rijke tube. This investigation is carried out in an attempt to explain the coupling that exists in such an environment between heat addition, pressure and velocity oscillations. Similar coupling may exist in various pulse combustion engines and unstable rocket motors. Due to inherent model complexities, there appears to have been no direct attempts in the past to approach this particular problem numerically. The present modeling employs unsteady, compressible, two dimensional flowfields that incorporate heat addition and acoustic interactions. The results show a relationship between pressure, velocity and heat transfer oscillations. As one might expect, heat transfer oscillations are found to be directly dependent upon the product of acoustic velocity and pressure. A possible explanation of the heat transfer mechanisms causing heat driven oscillations is offered in view of the computational findings. Due to the absence of complete analytical theories regarding this particular subject, the current numerical solution is hoped to serve as a base upon which a well-formulated theory could rely.

Nomenclature

a_0 = mean speed of sound inside the Rijke tube
A = oscillatory pressure amplitude
A_{obs} = surface area of obstacle or heater element
C_p = constant pressure specific heat
$\overline{h}$ = heat transfer coefficient
l = internal tube length
m = longitudinal oscillation mode, $m = 1,2,3,\ldots$
$p^{(1)}$ = oscillatory pressure component
Q = heat
q = heat transfer rate, dQ/dt
$q^{(1)}$ = oscillatory heat transfer rate
T = temperature
t = time
$u^{(1)}$ = oscillatory velocity component
x = axial distance from the bottom-end
γ = mean ratio of specific heats
λ = acoustic spatial wavelength
ρ = air density
ω = circular frequency, $m\pi a_0 / l$

Subscripts
in = refers to an incoming quantity
obs = refers to the obstacle or heat source
out = refers to an outgoing quantity
∞ = surrounding mean flow condition

Superscripts
(0) = denotes a steady or mean component
(1) = denotes an unsteady/oscillatory component

Introduction

The Rijke tube has been investigated both experimentally and theoretically[1-9]; however, none of the previous investigations offered a detailed explanation of the heat transfer mechanisms causing the heat driven oscillations. Due to the model complexity, there has been no pervious attempt to approach the problem numerically. Due to the lack of sufficient experimental data that can be used to verify or validate the semi-analytical formulations, and due to the absence of numerical results, most theories have remained limited and incapable of explaining the observed phenomena. For those reasons, the focus of this investigation will be to model the Rijke tube numerically, hoping to provide additional information and explain some of the observed phenomena. We also hope that the results of this study could be used to pave the way to more accurate theoretical formulations.

The present analysis begins with a brief classification of three types of pulse combustors, followed by a description of the self-excited oscillator that defines the character of the Rijke tube. Next, the computational model is presented, followed by a discussion of the key

*Group Scientist, Andrulis Corporation, Member AIAA.
†Professor, Department of Mechanical Engineering. Senior Member AIAA.
‡Assistant Professor, Department of Mechanical and Industrial Engineering. Member AIAA.

results. The numerical results will be shown to be in accord with existing experimental and theoretical predictions to the point of providing useful tools and detailed flowfield descriptions that tend to clarify existing speculations and furnish new means to improve existing analytical models. In relation to solid and hybrid rocket motors, they will predict a strong coupling between heat transfer fluctuations and fluctuations in the pressure and velocity fields that is particularly significant in the forward half of the motor.

Classification

The so-called pulse combustors[10] that have been developed to date can be divided into three categories according to their operational system geometry. These are: 1) the Schmidt tube (closed-open, quarter-wave system), 2) the Helmholtz resonator (closed-open or open-open system), and 3) the Rijke tube (open-open, half-wave system).[10]

The Schmidt tube that was developed in Germany[11] can be generally divided into three sections: 1) the inlet, 2) the combustion chamber, and 3) the tail or exhaust pipe (see Fig.1). The inlet section consists of one-way valves which open or close depending on whether the combustor pressure is lower or higher than the pressure upstream of the valves.

The Helmholtz resonator[12] consists of a rigid-wall cavity which has at least one short and narrow neck through which the enclosed fluid can communicate with the external medium (see Fig. 2). Due to the neck effect, the size of the device is less than a quarter of a wavelength.

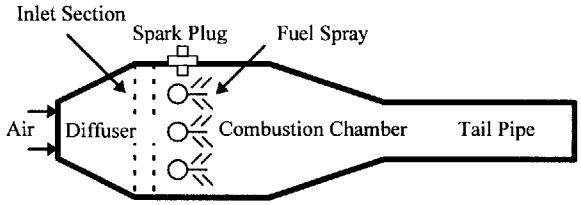

Fig.1 Schematics of a Schmidt tube pulse jet engine.

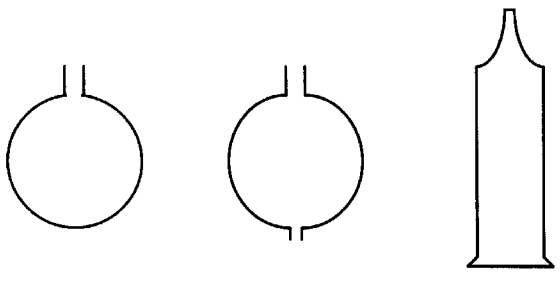

Fig. 2 Simple Helmholtz resonators.

The third type of pulse combustors is the Rijke tube where a heat source in the lower half of a vertical tube results in acoustic mode excitation.

Rijke Tube

Among the first accounts of thermoacoustical oscillations is that of Rijke[1] in 1859. In his work, Rijke discovered that strong oscillations occurred when a heated wire screen was placed in the lower half of an open-ended vertical pipe shown schematically in Fig. 3. Reported acoustic oscillations were found to stop altogether when the top end of the pipe was sealed, indicating that upward convective air currents in the pipe were essential for thermoacoustically driven oscillations to take place. As could be inferred from Fig. 3, the Rijke tube is a half wave pulse combustor since the acoustic wavelength is actually twice the length of the tube. From experimental reports, oscillations reached maximum amplification when the heater was located at the middle of the bottom half. At that location, both acoustic pressure and velocity are non-zero. For heater positions in the upper half of the pipe, damping instead of driving occurred. Rijke believed that rising convection currents expanded in the region of the heated screen and compressed downstream

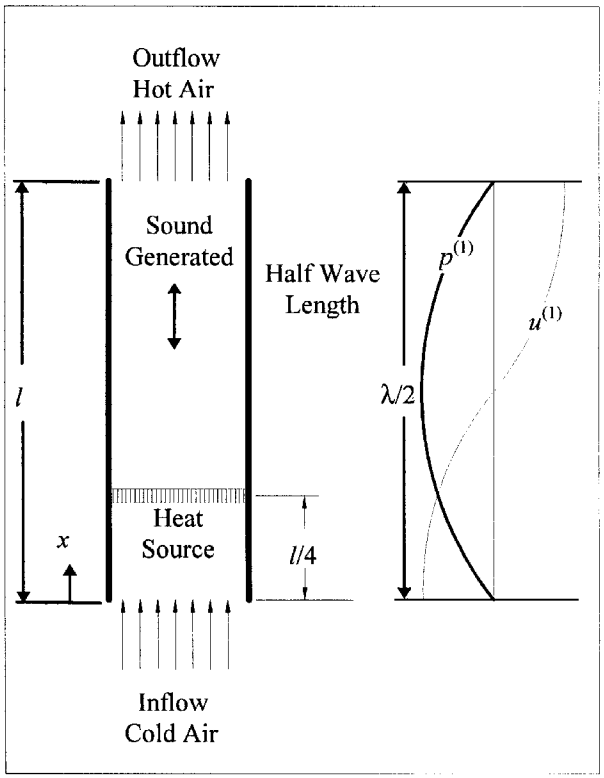

Fig. 3 The Rijke tube and associated fundamental acoustic wave structure.

from the heater due to cooling at the pipe walls. Accordingly, production of sound was attributed to successive expansions and contractions. This explanation remained limited since it could not address the details of heat exchange mechanisms causing the actual oscillations.

Since Rijke's discovery, there has been a number of theoretical and experimental attempts to explain this phenomenon[1-9]. Lord Rayleigh[1] proposed a criterion, later named after him, in which he addresses the relationship between heat addition and sound waves. According to Rayleigh's criterion, energy is fed into an acoustic disturbance when heat is added to a sound wave at the high temperature phase of its cycle; conversely, energy is lost from a sound wave when heat is added at the low temperature phase (Fig. 4). Since compression in a sound wave is adiabatic, pressure and temperature fluctuations are in phase. As a result, heat addition during a positive pressure disturbance increases the amplitude of the sound waves. Clearly, an opposite effect is seen when the pressure disturbance is negative. This is similar to the effect of heat addition in thermodynamic cycles. When heat is added at the high pressure phase of a cycle, the system gains energy. In the Rijke tube, the grid (or heat source) heats the air around it causing it to rise. Acoustically induced particle displacements are therefore superimposed on the naturally convected flow. When acoustic particle displacements are positive upwards, fresh cold air crosses the heated grid, but when negative downwards, hot air passes through the grid. During the upward pass, maximum heat transfer occurs between the heat source and the air. Since the timing in the acoustic cycle is such that maximum heat transfer corresponds to a positive particle displacement with favorable pressure, an ideal situation for acoustic wave growth is established.

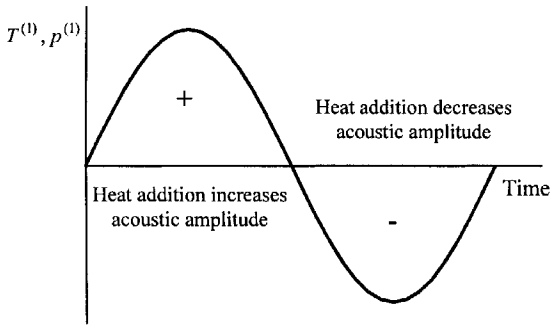

Fig. 4 Rayleigh's criterion.

If the grid is now placed in the upper half of the pipe, acoustic velocity and pressure have an unfavorable phase between them. Pressure acts adversely, in a direction that opposes particle motion. Under such unfavorable environment, acoustic amplification is not possible. A similar mechanism is used to explain the so-called reheat buzz, a jet engine instability of the reheat system (after-burner) which can be triggered in a similar fashion. There, acoustic velocity in a pipe disturbs the reheat afterburner flame and alters the rate of combustion. If the phase relationship between pressure and heat release rate is suitable, disturbances gain energy and grow in magnitude. Resulting pressure perturbations become large and lead to undesirable structural damage.

The Self-Excited Oscillator

The wave equation with the heat addition term acting as a driving function can be written for acoustic pressure and velocity as follows.[14]

$$\frac{1}{{a_0}^2}\frac{\partial^2 p^{(1)}}{\partial t^2} - \nabla^2 p^{(1)} = \frac{1}{C_p T^{(0)}}\frac{\partial q^{(1)}}{\partial t} \qquad (1)$$

$$\frac{\partial^2 u^{(1)}}{\partial t^2} - {a_0}^2 \nabla^2 u^{(1)} = -\frac{\gamma - 1}{\rho^{(0)}}\frac{\partial q^{(1)}}{\partial x} \qquad (2)$$

Equations (1) and (2) are characteristic of self-excited or "feedback" oscillations owing to the nature of the right-hand-side terms. Self-excited oscillations are different from the majority of oscillation-type problems in nature which are either of the free or of the forced type.

In a free oscillator, the amplitude decreases with time as a result of friction. In a forced oscillator, the energy associated with the motion is typically supplied by an oscillating force, an electric current or fluid flow or heat, which is modulated by the oscillator. This is the case in various mechanical clocks, electronic oscillators, musical wind instruments, bowed string instruments, the human voice, pulse combustions, and numerous types of whistles, control valves and pipes. In a forced oscillation, the sustaining alternating force exists independently of the motion and persists even when the oscillatory motion is stopped.

In a self-excited oscillation, the alternating force sustaining the motion is induced or controlled by the motion itself; when the motion stops, the alternating force disappears. Under certain conditions, the motion of an oscillator generates disturbances which can be fed back to the energy associated with the existing oscillations, acting effectively as a driving force. Such feedback can cause the amplitude to grow rather than

decay. Since the unsteady driving force $q^{(1)}$ that appears in Eqs. (1-2) is not externally controlled, but rather induced by fluctuations in other properties within the system, the Rijke tube is of the self-excited type.

As could be inferred from Eqs. (1-2), in order to seek analytical solutions to the problem and determine the oscillatory pressure and velocity distributions, the dependence of $q^{(1)}$ on the acoustic pressure and/or velocity must be known. Conditions controlling the flowfield on both sides of the heat source must also be known. For such reasons, one of the primary goals of this study will be to determine the form of $q^{(1)}$, relating it to $p^{(1)}$, $u^{(1)}$, or both.

A literature search has revealed that no exact closed form expression relating $p^{(1)}$, $u^{(1)}$, and $q^{(1)}$ has ever been derived. Computationally, no numerical technique has ever been attempted to extract information that can be exploited to achieve a better understanding and characterization of the peculiar coupling mechanism associated with the primary variables. In the remainder of this work, a theoretical explanation of the coupling mechanism will be sought via numerical analysis in an attempt to unveil the true character of the coupling mechanism and, particularly, to establish a functional dependence relating $p^{(1)}$, $u^{(1)}$, and $q^{(1)}$.

The Computational Model

The two-dimensional unsteady flowfield inside the Rijke tube has been computed with FLOW-3D developed by Flow Science Corporation.[15]

The pipe is 90 centimeters in length and has an internal diameter of 5 centimeters. Only one cross section of the pipe is modeled, thus taking advantage of prevalent geometric symmetry (since the pipe is a body of revolution and material properties, boundary conditions and other effects are symmetric with respect to the centerline). This problem consists of modeling a hollow cylinder inside a box. The hollow cylinder represents the Rijke tube and the box itself represents the room. Figure 5 gives a three-dimensional rendering of the Rijke tube inside the room. The computational mesh for the domain representing half of the Rijke tube and room in the x-z directions is defined in Fig. 6. The ambient atmospheric conditions, including pressure, temperature and density, are used to define the initial conditions at pipe inlets and outlets and inside the box. Air properties at standard sea level are used to calculate the density, thermal conductivity, specific heat, gas constant, and dynamic viscosity.

A solid porous obstacle with a diameter of 3.75 cm is added inside the tube at a location of 22.5 cm from the bottom-end to model the heat source. An obstacle porosity value of 0.9 was used which represents a 90 percent open area. Thermal conductivity, density, and heat capacity of steel were used to specify the obstacle properties. Heat had to be released inside the obstacle (at the source) with a time step shown in Fig. 7, since releasing the heat suddenly (say, at $t = 0$ sec) causes the program to crash.

Numerical Strategy

The numerical strategy consists of two stages reminiscent of transient and steady-state stages. The first stage carries the problem from an initial state of rest to a time of 20 seconds. After the first 20 seconds the problem reaches a terminal condition characterized by the presence of constant amplitude oscillations.

The second stage carries the problem from 20 seconds to 20.025 with a much smaller time interval in order to track more precisely the progressive acoustic wave growth. Virtual probes are located inside the Rijke tube model at numerous axial locations in order to monitor pressures, temperatures, densities and velocities. Primary input variables into the preprocessor are summarized in Table 1 below.

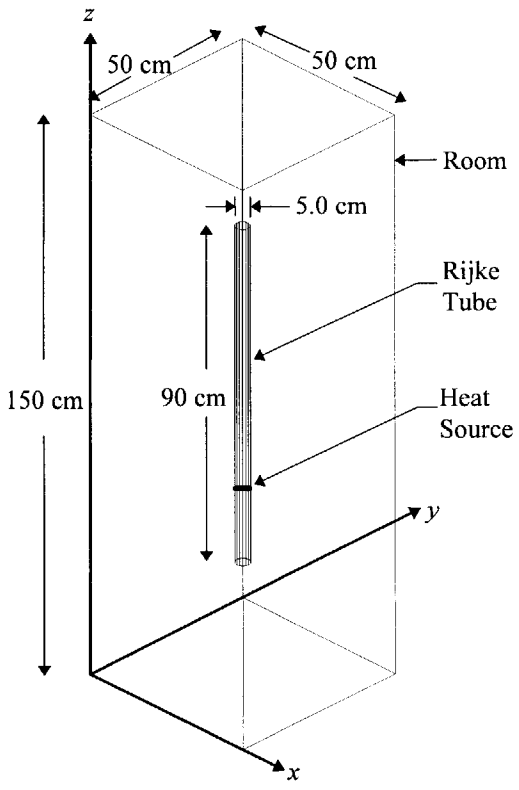

Fig. 5 Three-dimensional representation of the Rijke tube inside a room.

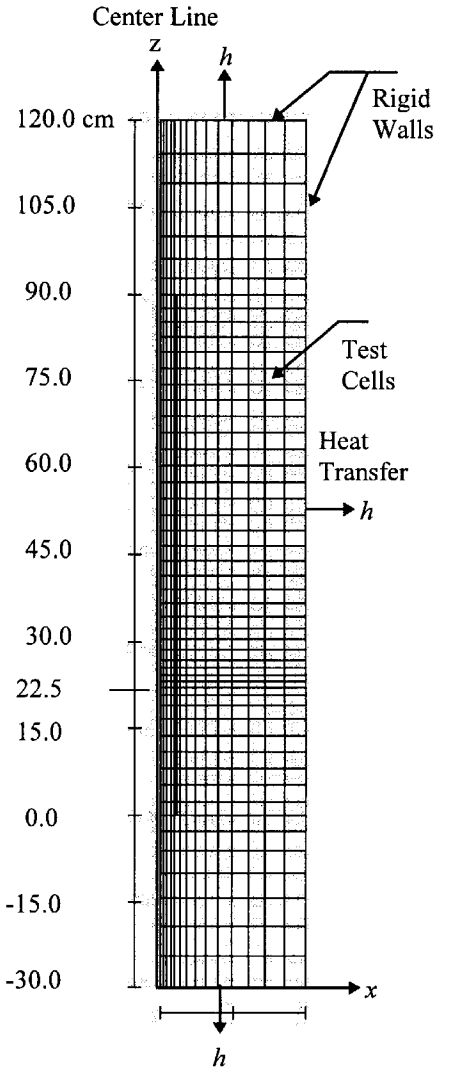

Fig. 6 Computational mesh.

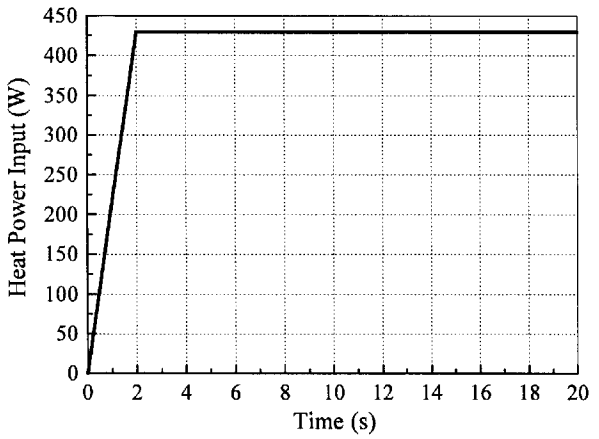

Fig. 7 Heat input at the source as a function of time.

Results and Discussion

The symmetric flowfield inside the Rijke tube has been computed with FLOW-3D using the full compressible flow option. The results will be presented in several separate sections. Discussion of each topic will be addressed as pertinent results are presented.

Standard Run

For the standard conditions described in Table 1 (corresponding to standard pipe properties, standard heat source, and standard gas properties), 430 watts of heat are released inside the tube at a location of $l/4$ from the bottom.

As the source temperature starts to rise, it produces a temperature difference between the source and the surrounding air. As a result, the local air density is reduced, causing air to be displaced in a convective cur-

Table 1 Standard input properties

	Unit	Input
Standard Pipe Properties		
Material	-	Steel
Diameter	cm	5
Length	cm	90
Wall thickness	cm	0.5
Thermal conductivity	W/m/K	36
Density-heat capacity product	$J/m^3/K$	$3.77x10^6$
Heat transfer coefficient	$W/m^2/K$	Calculated
Initial temperature	K	293.0
Standard Obstacle Properties		
Material	-	Steel
Diameter	cm	3.75
Thickness	cm	1.0
Location from bottom	cm	22.5
Porosity	-	0.9
Power input	W	430
Thermal conductivity	W/m/K	36
Density-heat capacity product	$J/m^3/K$	$3.77x10^6$
Heat transfer coefficient	$W/m^2/K$	Calculated
Initial temperature	K	293.0
Standard Gas Properties		
Gas medium	-	Air
Gas constant	J/Kg/K	287
Dynamic viscosity	kg/m/s	$1.824x10^{-5}$
Specific heat	J/kg/K	718
Thermal conductivity	W/m/K	0.0251
Initial temperature	K	293.0

rent. The heat transferred from the source to the surrounding air is a function of source temperature, ambient air temperature, source area, and average convection heat transfer coefficient, as given by Newton's cooling law:

$$q_{out} = \bar{h} A_{obs} \left(T_{obs} - T_{\infty} \right) \tag{3}$$

Figure 8 is a graphical representation of the pressure, radial velocity, axial velocity, temperature, density and source heat transfer versus time for the first 20 seconds. It shows that, after about 8.5 seconds, heat, pressure, and velocity oscillations begin. This coincides with the time when the air temperature around the source approaches its terminal condition characterized by a leveling out of the temperature curve (Fig. 8d).

Figure 9 shows the pressure, radial velocity, axial velocity, temperature, density and source to fluid heat transfer versus time for the second stage (20 to 20.025 sec) using a smaller time step to track the acoustic wave growth more accurately. This figure indicates that periodic oscillations are present in all the variables with a frequency of about 200 Hz which matches very closely the predicted natural frequency of the pipe given by $f = ma_0 / (2l)$.

Figure 10 shows the pressure and axial velocity oscillations at various locations along the pipe. An examination of Fig. 10a shows that pressure oscillations reach their maxima at the center of the pipe and minima at both ends. It also shows that pressure oscillations are in phase at any axial location, as one would expect from acoustic wave theory. Figure 10b, on the other hand, shows that velocity oscillations reach their maxima at both ends and are at a minimum at the center of the pipe. The velocity oscillations are 180° out of phase in the lower and upper half-domains.

These results exhibit the expected pattern predicted by acoustic theory, eliminating the possibility of being the mere outcome of computational error. They also agree with experimental observations in Rijke tubes.[1-5]

Conditions at the Upper and Lower Sides of the Source

Figures 11-13 show the pressure, temperature and density distributions along the length of the tube. The numerical data provides, for the first time, complete information regarding the flow properties, especially, at both ends of the heat source. Such information is necessary for setting up the boundary conditions that are needed to formulate an analytical model that allows determining $p^{(1)}$, $u^{(1)}$, or $q^{(1)}$. As one would expect, the steady pressure (in Fig. 11) is almost constant along the pipe. The temperature (in Fig. 12) remains constant in the lower section of the tube; it experiences a sudden jump crossing the source location; it then decays exponentially above the source. The density variation, plotted in Fig. 13, shows that the air expands after passing through the heat source. This similar but inverted dependence, by comparison to the temperature variation, is expected from the ideal gas equation.

Effect of Source Location

The location of the source is a key factor in producing oscillations inside the Rijke tube. When the source is placed in the lower half of the pipe, large amplitude oscillations are seen to occur. The resulting oscillations are found to have the largest amplitudes when the source is located at $(l/4)$ from the bottom end. This is in accord with experimental findings done previously.[1-5] During separate runs, the source was relocated to the middle $(l/2)$, and to the upper section $(2l/3)$ of the pipe in order to observe whether or not the oscillations would occur.

Figures 14-15 are graphical representations of the pressure, radial velocity, axial velocity, temperature, density and source heat transfer versus time at the $(l/2)$ and $(2l/3)$ source locations. The results indicate that when the source is positioned at $(l/2)$, where the amplitude of the pressure oscillation is maximum (corresponding to zero velocity), no oscillations are seen. The same can be said when the source is at $(2l/3)$, where the amplitude of velocity oscillations is a maximum (corresponding to zero pressure). It is observed that oscillations occur only when the product of the velocity and pressure is positive, and maximum when this product is a maximum as well. Figure 16 shows the temperature distribution of the source versus time at various locations. It is encouraging to see that the heat source has a lower temperature when placed at $(l/4)$ than at $(l/2)$ and $(2l/3)$. This can be attributed to the larger transfer of energy to the acoustic waves when the source is located at $(l/4)$ where heat conversion into acoustic energy is optimized.

Effect of Heat Input to the Source

For the standard conditions several different heat inputs (125.5, 376.6, 408.0, 426.9, 430.0, 433.1, and 439.4 watts) were released at the source at $(l/4)$ in order to examine the effect of varying the heat input on the induced acoustic motion.

Figure 17 is a graphical representation of the pressure, radial velocity, axial velocity, temperature, density and source heat transfer versus time for the first 20 seconds. Figure 17a (125.5 watts of heat input) does not show any sign of oscillations in the tube. This is an indication that the heat input level, which feeds the

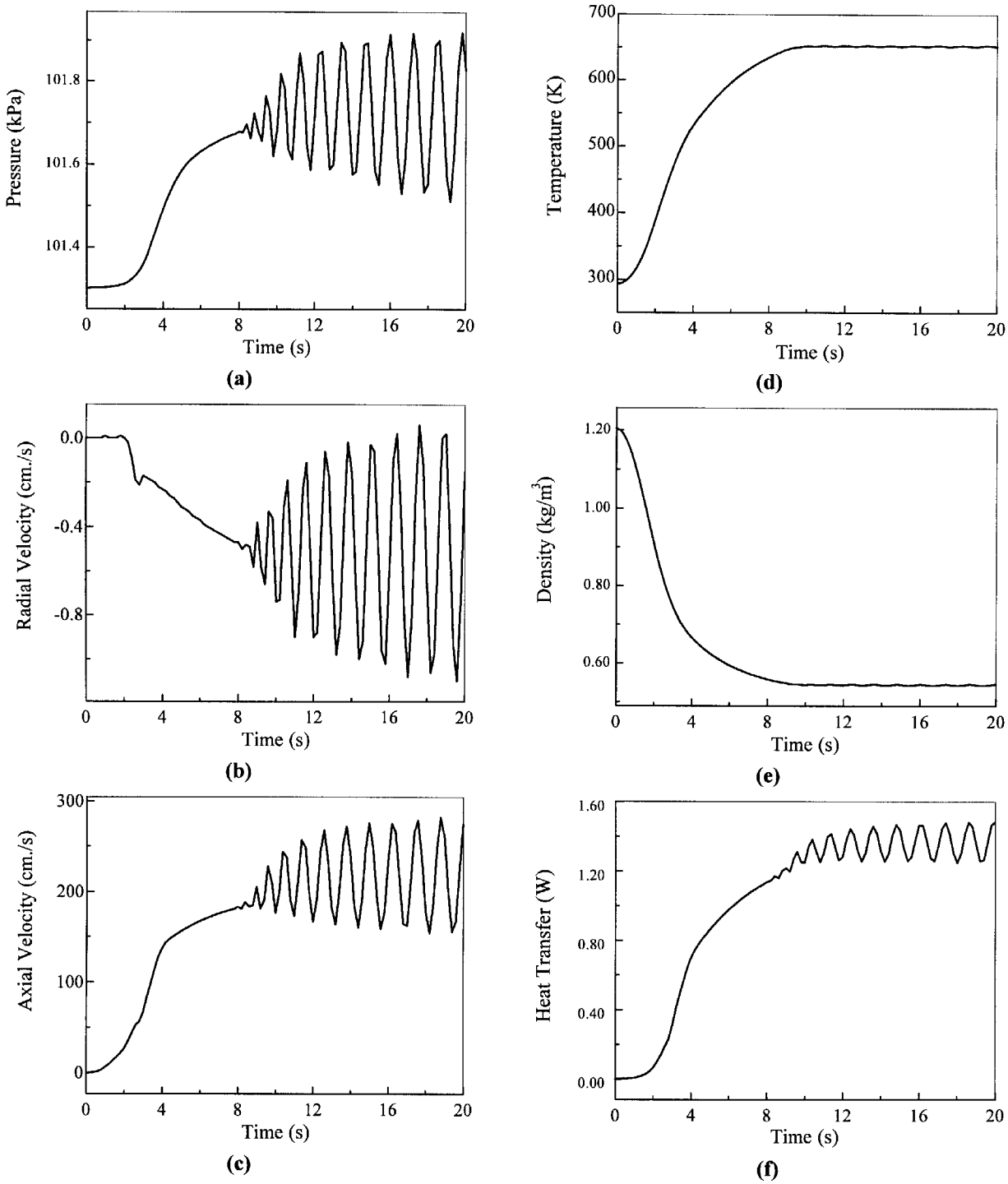

Fig. 8 Time-dependent (a) pressure, (b) radial velocity, (c) axial velocity, (d) temperature, (e) density, and (f) heat transfer versus time during the first 20.0 seconds (Stage I). This a standard run with 430 watts at the heater location which coincides with the virtual probe at *l / 4*.

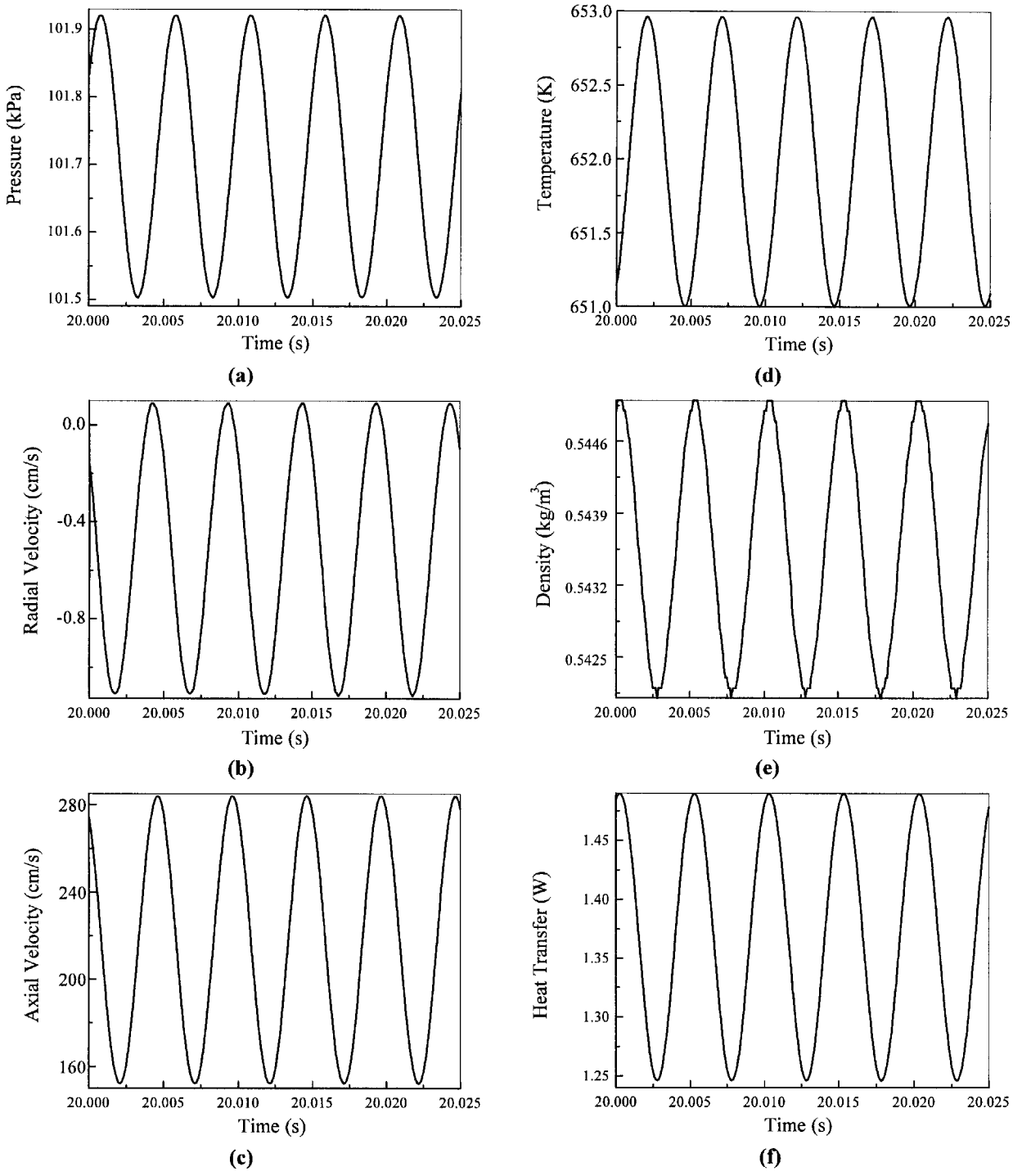

Fig. 9 Time-dependent (a) pressure, (b) radial velocity, (c) axial velocity, (d) temperature, (e) density, and (f) heat transfer versus time at a time step of 0.0025 seconds (Stage II). This a standard run with 430 watts at the heater location which coincides with the virtual probe at *l / 4*.

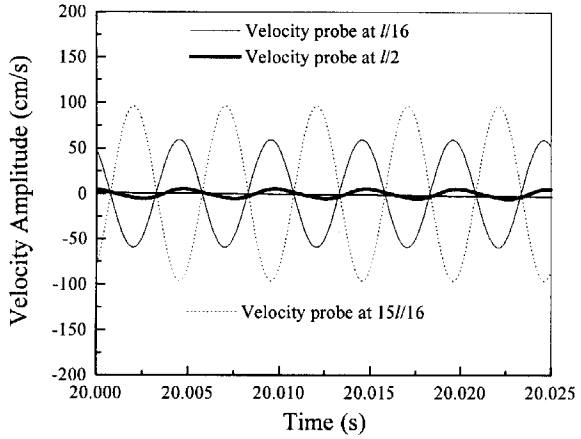

(a)

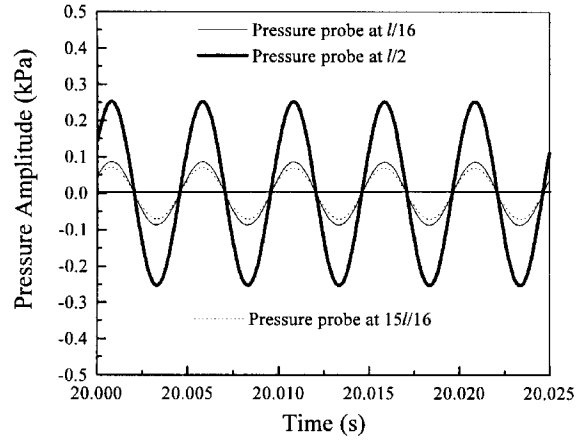

(b)

Fig. 10 (a) Pressure, and (b) axial velocity oscillations at various locations along the pipe versus time (Stage II).

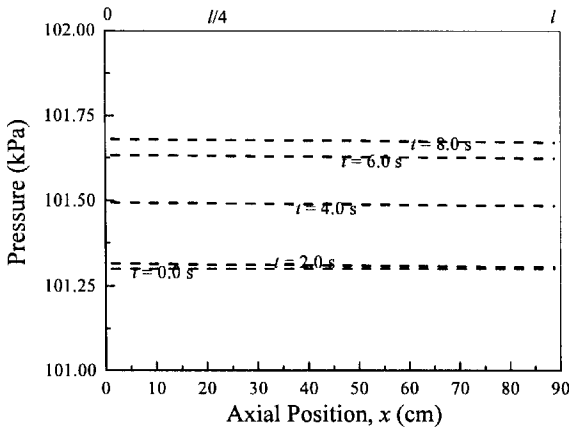

Fig. 11 Steady pressure at various times before the onset of oscillations (Stage I).

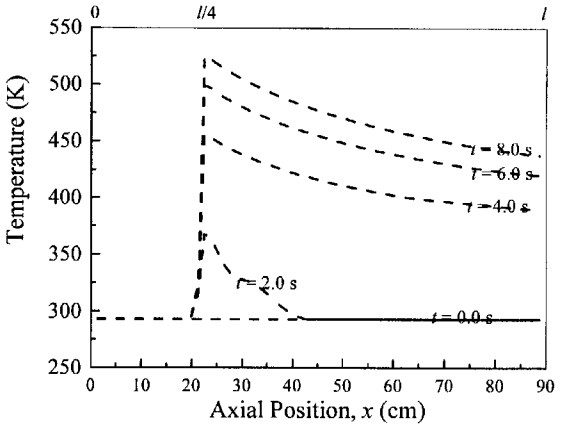

Fig. 12 Steady temperature at various times before the onset of oscillations (Stage I).

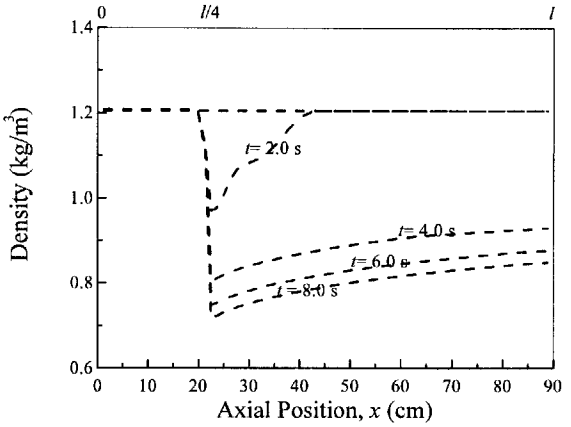

Fig. 13 Density at various times before the onset of oscillations (Stage I).

acoustic oscillations, has a threshold value. Figures 17b-17d show the presence of oscillations in the tube for heat inputs ranging from 376.6 to 426.9 watts. Figures 17e-f demonstrate that exceeding certain critical values of heat input triggers an instability characterized by growing acoustic wave amplitudes.

Figure 18 provides a trace of maximum pressure magnitudes at the various heat inputs. Pressure oscillations appear to grow exponentially with increasing heat input.

Pressure, Velocity and Heat Transfer Coupling

Figure 19 shows the pressure and velocity oscillations along the tube at different time periods during a cycle. Figure 19a shows that the pressure oscillation reaches its maximum amplitude at the center of the pipe and is minimum at both ends. This is in accord with plane-wave acoustic theory. Figure 19b shows that the velocity oscillation reaches its maxima at both ends and

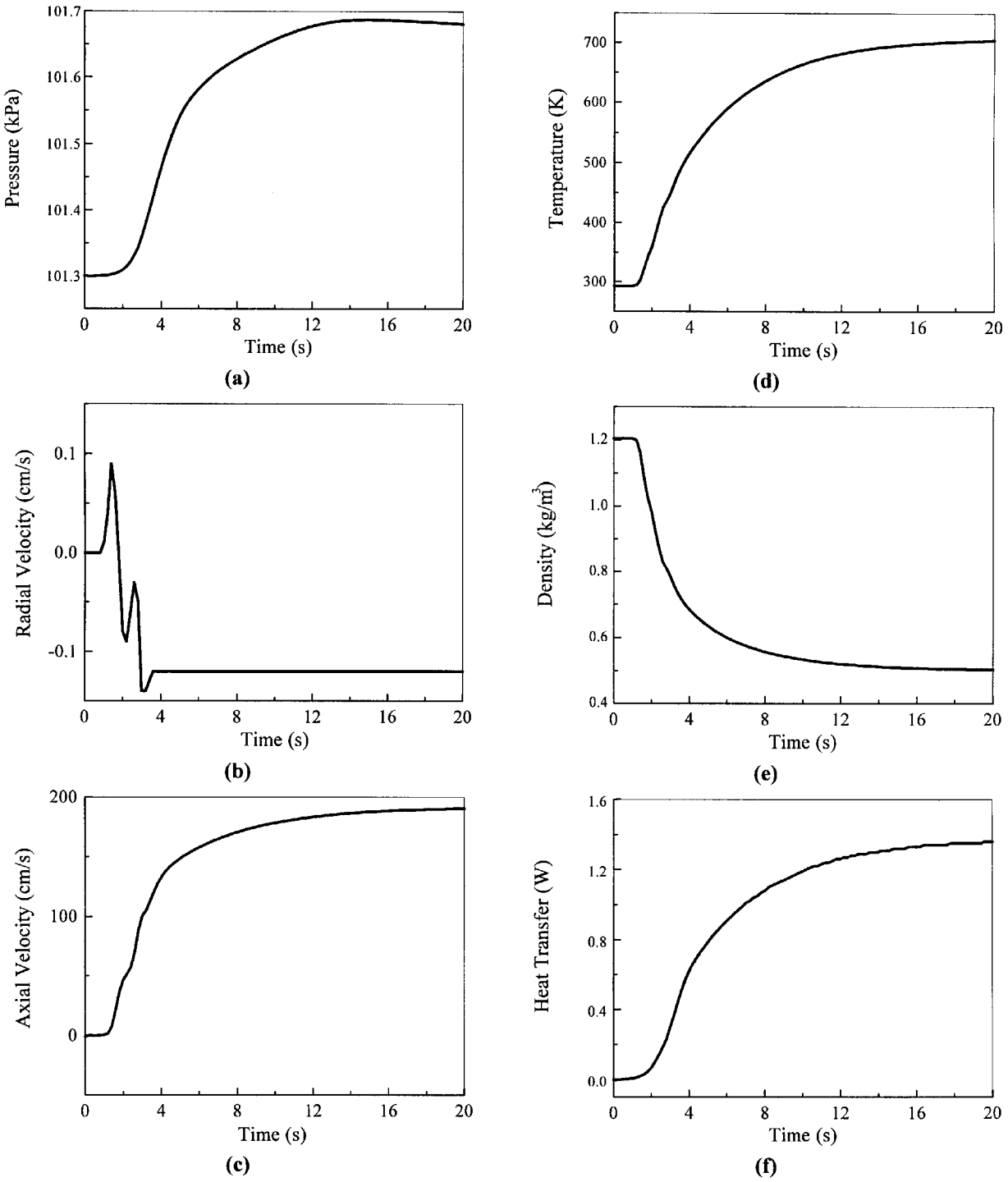

Fig. 14 Time-dependent (a) pressure, (b) radial velocity, (c) axial velocity, (d) temperature, (e) density, and (f) heat transfer versus time for the first 20.0 seconds. This a standard run with 430 watts at the heater location which coincides with the virtual probe at *l / 2*.

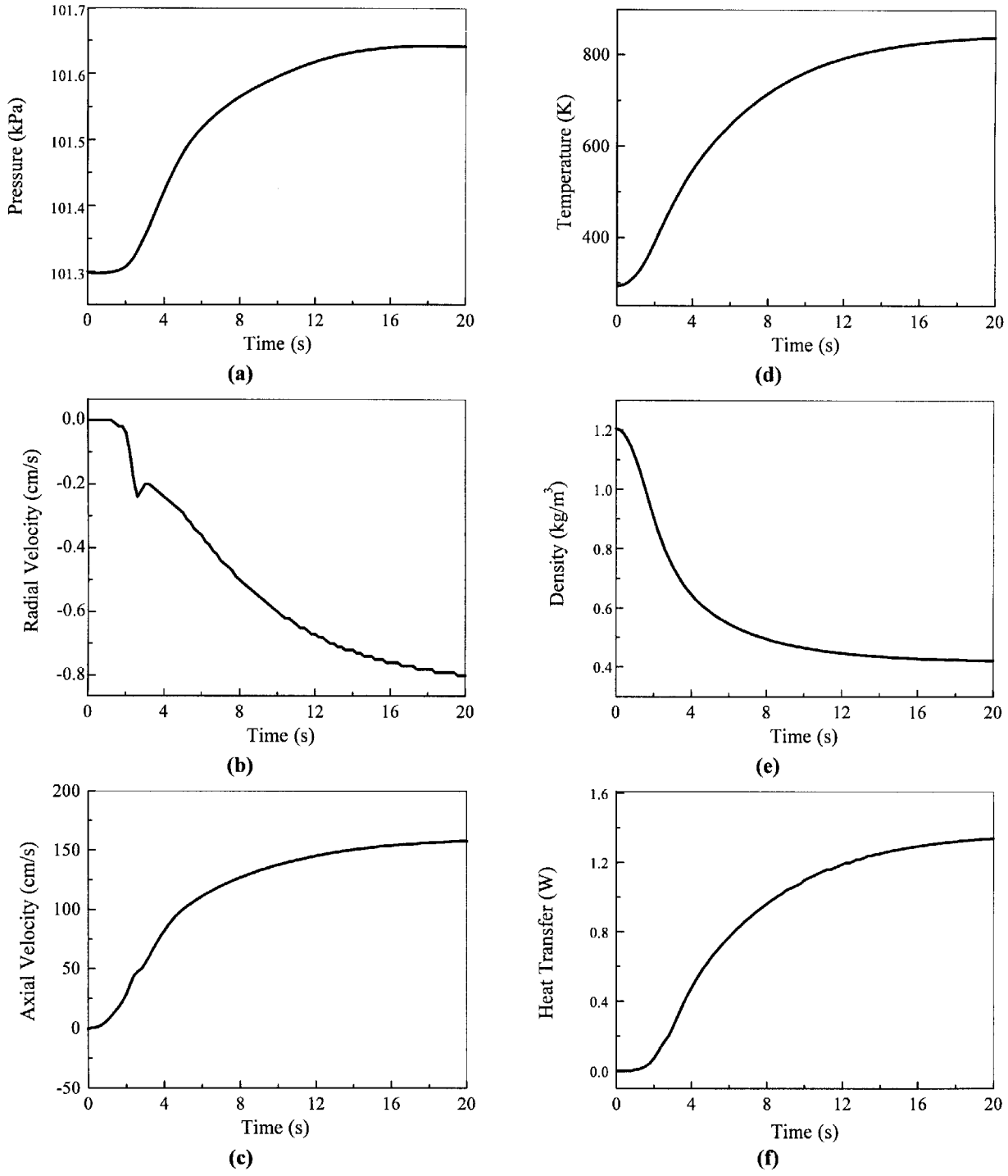

Fig. 15 Time-dependent (a) pressure, (b) radial velocity, (c) axial velocity, (d) temperature, (e) density, and (f) heat transfer versus time for the first 20.0 seconds. This a standard run with 430 watts at the heater location which coincides with the virtual probe at *2l / 3*.

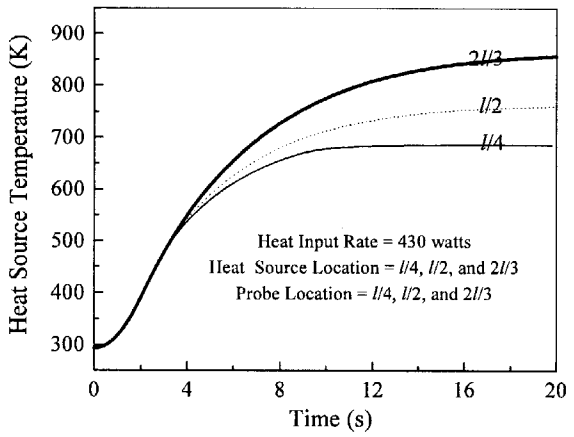

Fig. 16 Temperature of the source versus time at various locations.

is a minimum at the center of the pipe. This is also in agreement with acoustic theory. An interesting result is also seen in Fig. 19b which shows a jump in velocity amplitude right at the source location. This can be attributed to the strong local coupling between velocity and heat release at the source.

The Acoustic Phase Angles

Figure 20 shows the relationship between pressure, velocity and heat transfer oscillations at the source location. The pressure oscillation is leading the velocity oscillation by 90° and the heat oscillation is leading the velocity oscillation by 45° and lagging the pressure oscillation by 45°. This numerical phase result is in agreement with Carvallo's conclusions[5] that there should be a time lag between the fluid velocity and the heat transferred to the flow. Carvallo also concludes that, in general, the phase between the acoustic pressure and heat transfer cannot be 90°. This is in agreement with our result for a corresponding phase lag of 45°. In his study, Carvallo uses the following equation for pressure oscillations:

$$p^{(1)} = A\sin\frac{m\pi x}{l}\sin(\omega t + \phi) \qquad (4)$$

where ϕ, being the phase lead between $p^{(1)}$ and $q^{(1)}$, is left to be determined. From our numerical results, we concluded that $\phi = \pi/4$ in Eq. (4). This is a key result in assessing the relationship between pressure, velocity and heat oscillations. Using this newly found result, the time lag could be now incorporated into the expression for pressure.

The Form of Coupling

The current computational work shows that the magnitude of heat transfer oscillations is of the same order as the product of acoustic velocity amplitude, acoustic pressure amplitude, and the area of the source (see Table 2). This is indicative of a coupling between the acoustic heat transfer and the product of acoustic pressure and velocity in the standing wave field. Simply stated, it is a further indication of a direct conversion of acoustic intensity (mechanical energy) into heat and vice versa. An analytical expression for the heat transfer that satisfies existing criteria and conditions can be now proposed. This equation is:

$$q^{(1)} = Const \times p^{(1)}u^{(1)} \qquad (5)$$

Concluding Remarks

The numerical results described above, which agree with experimental observations, are supportive of a theory that attributes heat transfer coupling to the combined effects of pressure and velocity. Both experimental observations and present numerical solutions concur that, unless the product of pressure and velocity is positive, acoustic damping will occur. This leads us to believe that velocity or pressure alone cannot be solely responsible for driving the oscillations, convincing us to be in favor of a theory that proposes coupling between the unsteady components of pressure, velocity and heat transfer.

Acknowledgment

The authors would like to thank Dr. Michael Barkhudarov of Flow Science, Inc., for his help and support. Without his helpful contributions, this work would not have been possible.

References

[1]Rayleigh, J.W.S., *The Theory of Sound*, Vol. 1 and 2, Reprint of 1894-6 Edition, Dover Publications, New York, 1945.

[2]Zinn, B.T., Miller, N., Carvalho, J.A. Jr., and Daniel, B. R., "Pulsating Combustion of Coal in a Rijke Type Combustor," Proceedings, 19th International Symposium on Combustion, 1982.

[3]Evans, R.E., and Putnam, A.A., "Rijke Tube Apparatus," *J. Appl. Phys.*, No 360, 1966.

[4]Collyer, A. A., and Ayres, D. J., "The Generation of Sound in a Rijke Tube Using Two Heating Coils," *J. Phys: Appl. Phys.*, Vol. 5, 1972.

[5]Carvalho, J.R., Ferreira, C., Bressan, C., and Ferreira, G., "Definition of Heater Location to Drive Maximum Amplitude Acoustic Oscillations in a Rijke Tube," *Combustion and Flame*, Vol. 76, 1989.

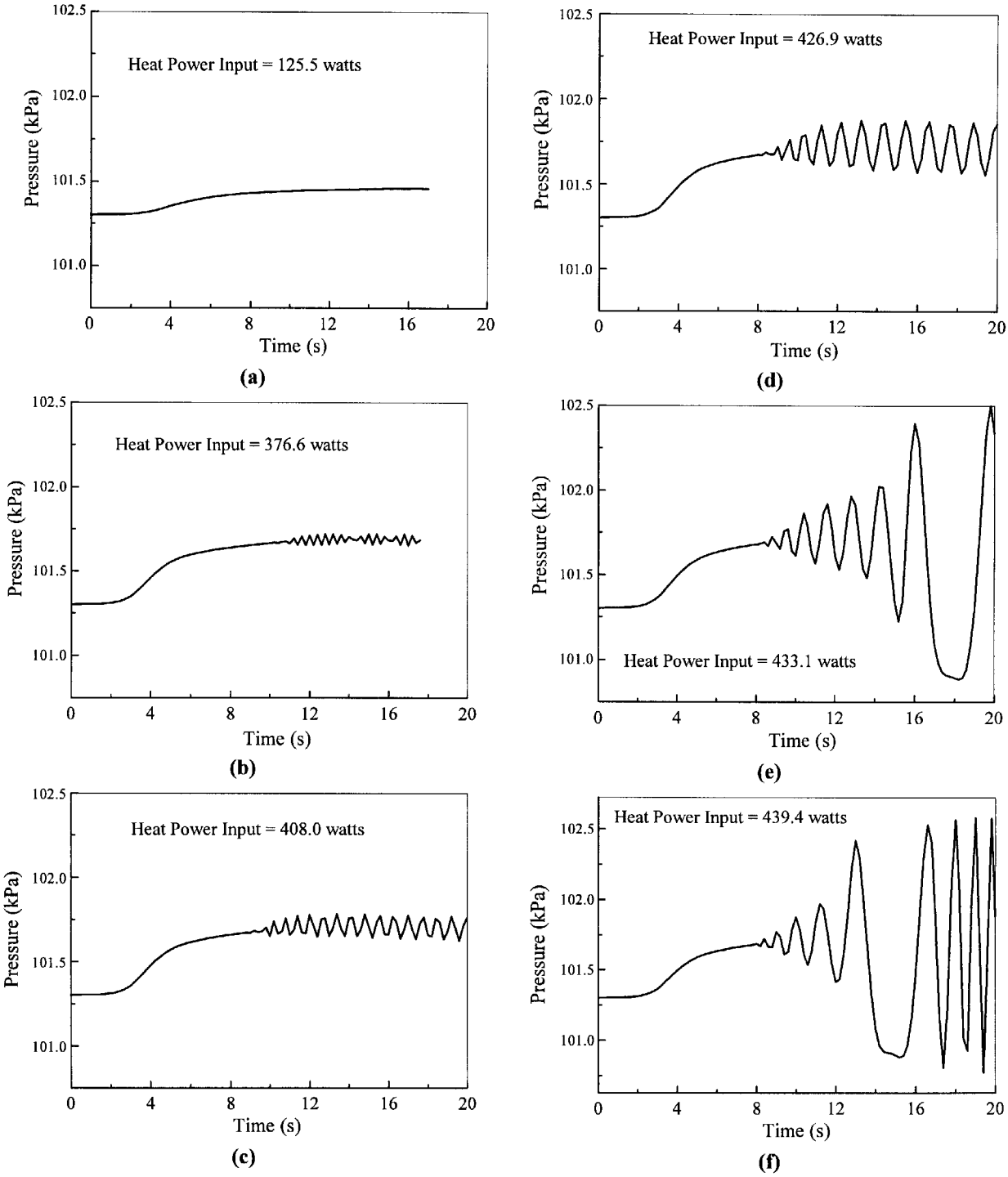

Fig. 17 Pressure versus time for different power inputs for the first 20 seconds (Stage I). This a standard run with a heater location that coincides with the virtual probe at *1 / 4*.

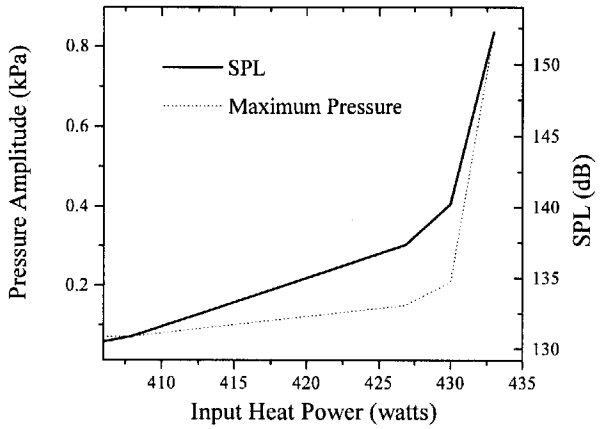

Fig. 18 Maximum pressure versus time at various heat power inputs.

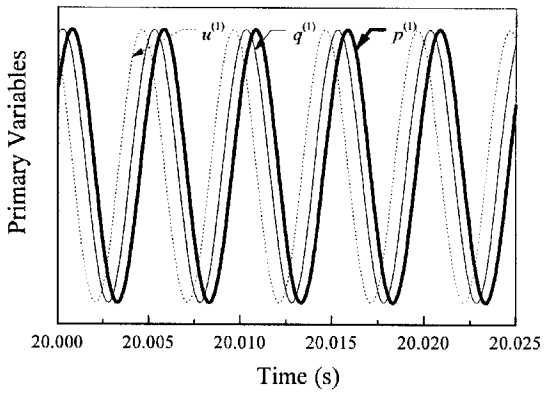

(a) During Stage II

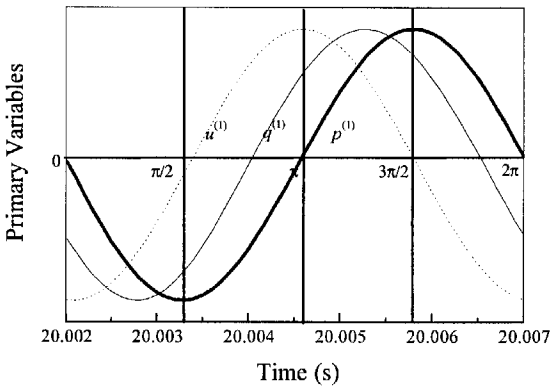

(b) During a cycle in Stage II

Fig. 20 Relationship between pressure, axial velocity and heat transfer oscillations at location *l / 4* versus time (Stage II).

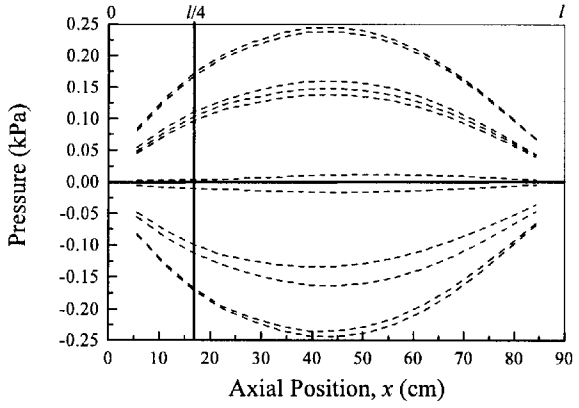

(a)

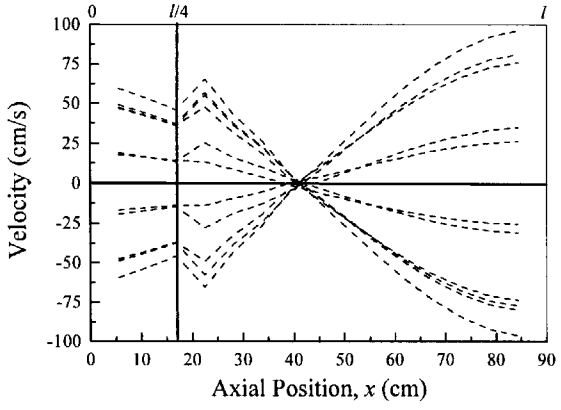

(b)

Fig. 19 (a) Pressure and (b) velocity versus axial length along the pipe at various time steps during one period.

Table 2 Coupling variables vs. heat power input

q_{in} (W)	A_{obs} (cm^2)	$p_{max}^{(1)}$ (Pa)	$u_{max}^{(1)}$ (m/s)	$A_{obs}p_{max}^{(1)}u_{max}^{(1)}$ (W)	$q^{(1)}$ (W)
125.5	11.03	-	-	-	-
376.6	11.03	33.65	0.0868	3.22×10^{-3}	18.7×10^{-3}
408.0	11.03	71.45	0.1856	1.46×10^{-2}	4.04×10^{-2}
426.9	11.03	151.25	0.3942	6.58×10^{-2}	8.62×10^{-2}
430.0	11.03	208.80	0.6586	0.152	0.12
433.1	11.03	837.20	2.622	2.42[a]	0.485
439.4	11.03	924.40	2.435	2.25[a]	0.491

[a] Corresponding to growing acoustic instability.

[6]Carrier, G.F., "The Mechanics of Rijke Tube," *Q. appl. Math.*, Vol. 12, 383, 1955.

[7]Maling, G.C., "Simplified Analysis of the Rijke Phenomenon," *Journal of the Acoustical Society of America*, Vol. 35, 1058, 1963.

[8]Miller, J. Carvalho, J.A.S., "Comments on Rijke Tube," *Scient. Am.*, No 204, 180, 1961.

[9]Friedlander, M.M., Smith, T.J.B., "Experiments on the Rijke Tube Phenomenon," *Journal of the Acoustical Society of America*, Vol. 36, 17, 1964.

[10]Zinn, B.T., "State of the Art and Research Needs of Pulsating Combustion," American Society of Mechanical Engineers, 84-WA/NAC-19, December 1984.

[11]AGARD, *History of German Guided Missiles Development,* First Guided Missiles Seminar, Munich, Germany, 1956.

[12]Kinsler, L.E., Frey, A.R., Coppens, A.B., and Sanders, J.V., *Fundamentals of Acoustics,* John Wiley and Sons, New York, 1982.

[13]Dowling, A.P., and Efows Williams, J.E., *Sound and Source of Sound,* Ellis Horwood limited, West Sussex, England, 1983.

[14]Chu, B.T., NACA RM 56D27, 1956.

[15]Flow Science Incorporated, Los Alamos, New Mexico.